We are IntechOpen,
the world's leading publisher of
Open Access books
Built by scientists, for scientists

4,800
Open access books available

122,000
International authors and editors

135M
Downloads

Our authors are among the

154
Countries delivered to

TOP 1%
most cited scientists

12.2%
Contributors from top 500 universities

CLARIVATE ANALYTICS

BOOK CITATION INDEX

INDEXED

WEB OF SCIENCE™

Selection of our books indexed in the Book Citation Index
in Web of Science™ Core Collection (BKCI)

Interested in publishing with us?
Contact book.department@intechopen.com

Numbers displayed above are based on latest data collected.
For more information visit www.intechopen.com

The Composition Effect on the Dynamics of Electrons in Sb-Based QD-SOAs

B. Al-Nashy[1] and Amin H. Al-Khursan[2]
[1] Science College, Missan University, Missan,
[2]Nassiriya Nanotechnology Research Laboratory (NNRL),
Science College, Thi-Qar University, Nassiriya,
Iraq

1. Introduction

In 1961, it is suggested that stimulated emission can occur in semiconductors by recombination of carriers that are injected across a p-n junction. This is the backbone in the concept of semiconductor lasers and amplifiers [1]. This concept is connected with the "one dimensional electron in a box", a problem discussed by quantum mechanics text books, to generate a new field of confined semiconductor structures known thereafter as quantum-well (QW), quantum-wire (QWi) or quantum dot (QD) structures where the carriers are confined in semiconductor in one, two, or three directions, respectively [2]. Semiconductor optical amplifiers (SOAs) and lasers performance may be substantially improved by using the QD-SOAs characterized by a low threshold current density, high saturation power, broad gain bandwidth and week temperature dependence as compared to bulk and multi-quantum well devices [3]. QD active region results from reducing the size of conventional (bulk) crystal to a nanometer size scale in all the crystal directions. This results in a complete quantization of energy states. The density of states becomes comparable to a delta-function. In order to cover losses of the waveguide of the SOA, QDs are then grown by a large number of dots grown on a WL which is already in the form of QW layer, see Fig. 1.

In this chapter, we examine the effect of changing composition of the layers constructing the Antimony (Sb)- based quantum dot semiconductor optical amplifiers (QD-SOAs). We start-off in sections 2-3 a general description of QD-SOA and the importance of SOAs, especially Sb-based SOAs, in solving problems. Manufacture imperfection in the shape of QDs are taken into account in the gain calculations in section 4, where they are represented by an inhomogeneous function. Along with the gain description in this section, a global Fermi-function is used where the states in the barrier layer, wetting layer (WL) and ground and excited states of the dots are included in the calculations of Fermi-energy. This mathematical formulation coincides with our subject of study since we would like to see the effect of all the QD-SOA layers. QD-SOA is modeled in section 5 using rate equations (REs) model for the barrier layer which is assumed to be in the form of separate confinement heterostructure layer (SCH), wetting layer (WL), ground state (GS) and excited state (ES) in the QD region of Sb-based structures and then solved numerically. A 3 REs model is discussed first where the

barrier SCH layer is neglected in this model, as done in many literatures, then a 4 REs model is described, where the SCH layer is included. Sb-based QD-SOA structures, the matter of study, are described in detail both in the shape and composition in section 6. Results of the calculations from these models are described in detail in section 7 where the material confinement is examined through the changing of Sb-composition in the QD, WL and SCH layers and it is shown to affects QD-SOA gain and dynamics. Changing WL composition affects the dynamics of ES and GS. InSb dots are shown to be more appropriate for inline static amplification. Results from 3 REs model overestimates the carrier dynamics in comparison with 4 REs calculations. Thus, the SCH barrier layer must be included in the RE models for convenient description of the processes in the QD-SOA. Our results supports the importance of inclusion global quasi-Fermi energy in explaining the results. Finally, section 8 concludes the main finding from this chapter.
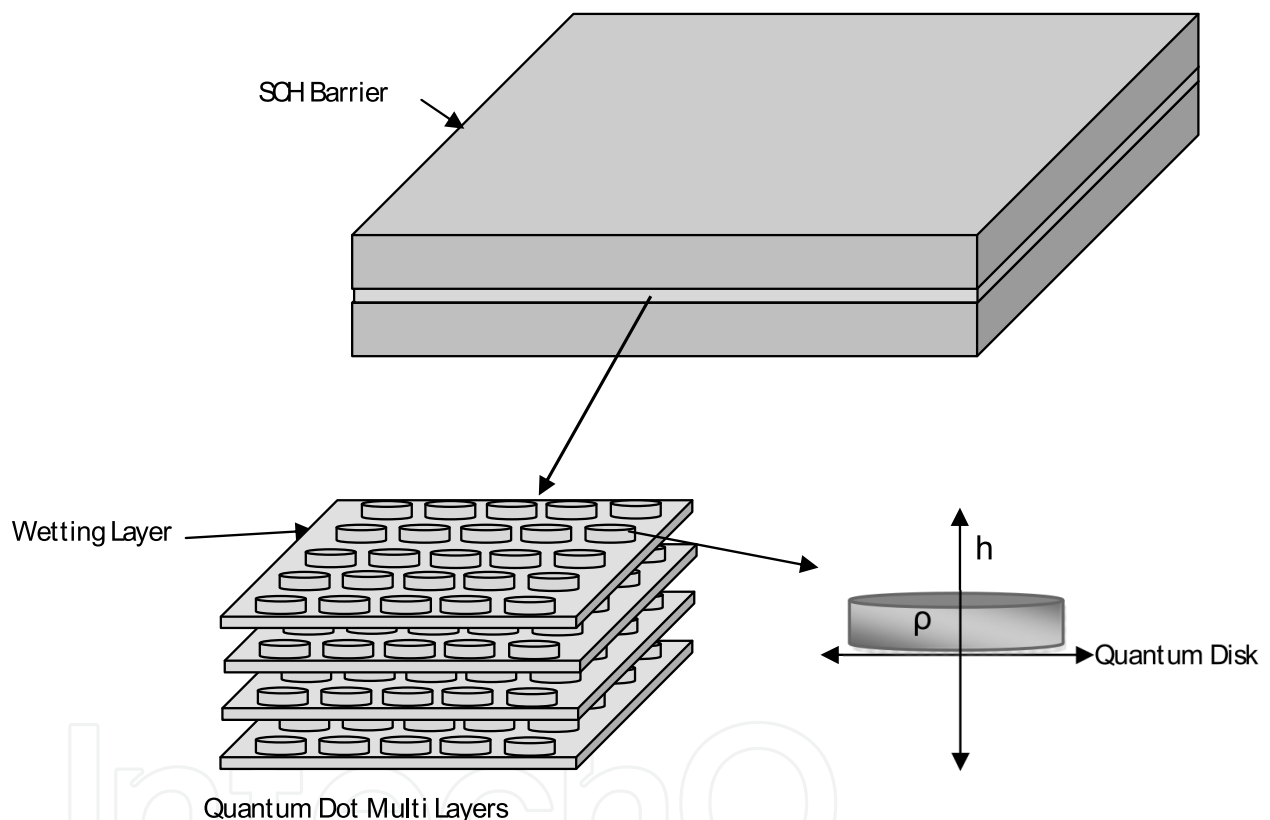

Fig 1. Schematic illustration of the QD active layer which consists of an arrays of Quantum Disks grown on an wetting layer covered by SCH barrier.

2. Semiconductor optical amplifier

Transmitters, receivers, electronic switches and routers limits the capacity of optical communication systems that can exceed 10 Tb/s by the speed of their electronic components [3]. Optical fibers suffers from attenuation (which limits transmission distance) and dispersion (leading to an increase in the system bit error rate, BER). 3R method (reshaping-retiming-retransmission) is then used to regenerate the optical signal in optical fibers. It has a number of disadvantages. This involves low optical and electrical transparencies in addition to network unreliability. These limitations may be overcome by using SOAs. The

electronic components can be replaced by ultrafast all-optical signal processing components. SOAs are among the most promising candidates for all-optical signal processing devices due to their high speed capability, low switching energy, compactness, and optical integration compatibility. In optical fibers, as the in-line amplifier has only to carry out one function (amplification of the input signal) compared to full regeneration, it is intrinsically a more reliable and less expensive device. Optical amplifiers can also be a useful as power boosters, for example to compensate for splitting losses in optical distribution networks. It can be used as optical preamplifiers to improve receiver sensitivity [3,4].

A semiconductor optical amplifier (SOA) is basically a semiconductor laser (gain medium) with a low feedback mechanism and whose excited carrier amplifies an incident signal but do not generate their own coherent signal. Thus, it operated as a broadband single-pass device for amplification. Each SOA requires some form of external power (a current or optical source) to provide the energy for amplification. An electrical current inverts the medium, by transferring electrons from the valence to the conduction band, thereby producing spontaneous emission and the potential for stimulated emission yields the signal gain. The first studies of SOAs were carried out around the time of the invention of the semiconductor laser in the 1960's. In the 1970's Zeidler and Personick carried out early work on SOAs. Research on SOA device design and modeling gets a lot of importance in 1980's especially for AlGaAs SOAs operating at (830 nm) wavelength and InGaAsP/InP SOAs operating in the (1300-1550 nm) region. In 1989 SOAs designed as devices uses a symmetrical waveguide structures giving much reduced polarization sensitivities [5].

3. Sb-based QD-SOA

Mid-to-far-infrared wavelength range (2000-30000 nm) has a variety of applications including remote sensing, medical diagnostic, free-space optical communications, atmospheric pollution monitoring, chemical sensing, thermal imaging, high power and mid-infrared light sources [6]. Although HgCdTe material is already used to build devices working at these ranges, it suffers from slow response, high-power dissipation and undesired noise [7]. III-Sb based devices appear as a counterpart, since it is offering several advantages such as wide spectral range, low electron effective mass and high mobility at room temperature [8]. Although its research begins since the 70s of the past century, Sb-based devices still need a lot of length of study especially when the active region is in the form of QD nanostructures. Using QD active region in the Sb-based devices adds the advantages resulting from QD nanostructures to that expected from the Sb-based infrared devices.

QD-SOAs can be used in the building blocks of many photonic devices. Its response is controlled by their dynamic behavior which can be studied by the use of a three-level system of REs to describe QD-SOA states for ground state (GS), excited state (ES) and WL state, which is considered as a QW and then can be approximated by a single state. While quasi-Fermi levels in the conduction and valence subbands are typically calculated from the surface carrier density per QD layer, now in some recent researches, both WL and barrier layer are included [9]. The barrier layer considered here is assumed to be in the form of a separate confinement heterostructure layer (SCH). This layer used in semiconductor structures to assure carrier confinement, where the SCH layer must have a high bandgap compared to other layers constructing the semiconductor device. Accordingly, the barrier layer becomes included in the gain calculations. Due to this, we begin in our laboratory

(NNRL) a series of studies for some of the characteristics of Sb-based QD devices [10]. Here, the carrier dynamics in III-Sb based QD-SOAs are considered using four-level REs system. QD, WL and SCH barrier compositions are examined to specify their characteristics. The results then, compared with those of three-level REs show the importance of including the barrier layer in the QD SOAs calculations. Because of the much larger effective mass of holes and lower quantization energies of the QD levels in the valence band, electrons behavior limits the carrier dynamics while holes in the valence band are assumed to be in quasi-thermal equilibrium at all times [11]. Thus, we determine carrier dynamics here by the relaxation of electrons in the conduction band only.

4. Inhomogeneous gain model with global quasi-fermi levels

Actually, QDs have imperfections in shape and randomly distributed on the substrate. These QDs emit photons at slightly different energies which results in an inhomogeneous broadening [11]. In our model, a Gaussian distribution function is used to describe inhomogeneous broadening. Accordingly, the linear gain of QD structures can be written as [9, 12]

$$g^{(1)}(hw) = c_0 \sum_i \int_{-\infty}^{\infty} dE' |M_{env}|^2 |\hat{e}.p_{cv}|^2 D(E')L(E',hw)[f_c(E',F_c) - f_v(E',F_v)] \qquad (1)$$

where $c_0 = \dfrac{\pi e^2}{m_0^2 \varepsilon_0 c n_b \omega}$, m_0 is the free electron mass, ε_0 is the permittivity of free space, c is the speed of light in free space, n_b is the background refractive index of the material, ω is the optical angular frequency of the injected optical signal and E' is the optical transition energy. $|M_{env}|^2$ is the envelope function overlap between the QD electron and hole states. The term $[|\hat{e}.p_{cv}|^2 = \dfrac{3}{2}(\dfrac{m_0}{6})E_p]$ is the momentum matrix element for electron-heavy hole transition energy in TE polarization, E_p is the optical matrix energy parameter. The Lorentzian line shape function $L(E')$ for gain is defined by

$$L(E',\hbar w) = \dfrac{\dfrac{\hbar \gamma_{cv}}{\pi}}{(E' - \hbar \omega)^2 + (\hbar \gamma_{cv})^2} \qquad (2)$$

With $\gamma_{cv}(=1/\tau_{in})$ is the intraband scattering rate. $D(E')$ is the inhomogeneous density of states of the self-assembled QD and is expressed as [13]

$$D(E') = \dfrac{\mu_i}{V_{dot}} \dfrac{1}{\sqrt{2\pi\sigma^2}} \exp\left(\dfrac{-(E' - E^i_{max})^2}{2\sigma^2}\right) \qquad (3)$$

where μ_i is the degeneracy of the ith state of a QD, $\mu_{GS} = 2, \mu_{ES} = 4$ for the ground state and the excited state, respectively. V_{dot} is the effective volume of the QDs. σ is the spectral variance of the QD distribution and E^i_{max} is the transition energy at the maximum of QD

distribution of the ith optical transition. The terms f_c and f_v are the respective quasi-Fermi level distribution functions for the conduction and valence bands, respectively. Recent researches [8] uses global states to describe the global quasi-Fermi levels F_c and F_v in the conduction and valence bands where the contributions to the Fermi-levels from the barrier layer and WL are included in addition to that from QDs. They are determined from the surface carrier density per QD layer by the following relations [13]

$$n_{2D} = N_D \sum_i \frac{s^i}{\sqrt{2\pi\sigma_e^2}} \int e^{-\left(E_c' - E_{ci}^D\right)/2\sigma_e^2} f_c\left(E_c', F_c\right) dE_c'$$
$$+ \sum_l \frac{m_e^W K_B T}{\pi\hbar^2} \ln\left(1 + e^{\left(F_c - E_{cl}^W\right)/K_B T}\right)$$
$$+ H_b \int \frac{1}{2\pi^2} \left(\frac{2m_e^B}{\hbar^2}\right)^{3/2} \sqrt{E_c' - E_c^B} f_c\left(E_c', F_c\right) dE_c' \tag{4}$$

$$p_{2D} = N_D \sum_i \frac{s^i}{\sqrt{2\pi\sigma_h^2}} \int e^{-\left(E_h' - E_{hj}^D\right)/2\sigma_h^2} f_v\left(E_h', F_v\right) dE_h'$$
$$+ \sum_m \frac{m_h^w K_B T}{\pi\hbar^2} \ln\left(1 + e^{\left(F_v - E_{hm}^w\right)/K_B T}\right)$$
$$+ H_b \int \frac{1}{2\pi^2} \left(\frac{2m_h^B}{\hbar^2}\right)^{3/2} \sqrt{E_h^B - E_h'} f_v\left(E_h', F_v\right) dE_h' \tag{5}$$

where n_{2D} and p_{2D} are the surface densities of electrons and holes per QD layer, respectively. E_{ci}^D and E_{hi}^D represents the respective confined QD states in the conduction and valence bands. σ_e and σ_h are the spectral variance of the QD electron and heavy-hole distributions, respectively. The term E_c' is the energy in the conduction band and E_h' is the energy in the valence band. Heavy hole subbands are included, only, in the calculations of valence subbands since light hole subbands are deep and can be neglected. k_B is the Boltzmann constant and T is the absolute temperature. The terms m_e^W (m_h^W) and E_{el}^W (E_{hm}^W) are the effective electron (hole) mass and the subband edge energy of the conduction (valence) band of WL. The term H_b is the thickness of SCH barrier. The terms m_e^B (m_h^B) and E_c^B (E_h^B) are the electron (hole) mass and the conduction (valence) band edge energy of barrier layer.

5. Rate equations of Sb-based QD-SOAs

5.1 Three rate equations model
QD-SOA characteristics can be studied using REs system constructed from three equations which describe the dynamics in WL, GS and ES of QD layer. The QD inhomogeneity due to

fabrication imperfections is introduced through gain as discussed in section 3 above. Examples of three REs system can be found in [11, 14]. In the three REs system, carriers are assumed to be injected with current density, J, in WL where the barrier layer effect is neglected. In WL, carriers are recombining at a rate $(1/\tau_{wR})$, relax at a rate $(1/\tau_{w2})$ to the ES. ES relaxes quickly to GS at rate $(1/\tau_{21})$, thus it does not contribute to gain. The escape component from ES to WL is $(1/\tau_{2w})$ and from GS to ES is $(1/\tau_{12})$. Both GS and ES are assumed to be recombining at the same rate $(1/\tau_{1R})$, see Fig. 2. The Pauli blockings $(1-h)$ and $(1-f)$ are taken for the nonempty ES and GS, respectively. For example, if ES is empty, then ($h=0$) and carriers can occupy the state, if it is fully occupied, then ($h=1$) and no further carriers can occupy it. The above described processes are represented by the following REs model for the carrier density N_w in the WL, occupation probabilities h and f in the ES and GS, respectively

$$\frac{\partial N_w}{\partial t} = \frac{J}{qL_w} - \frac{N_w(1-h)}{\tau_{w2}} + \frac{N_wh}{\tau_{2w}} - \frac{N_w}{\tau_{wR}} \tag{6}$$

$$\frac{\partial h}{\partial t} = \frac{N_wL_w(1-h)}{N_Q\tau_{w2}} - \frac{N_wL_wh}{N_Q\tau_{2w}} - \frac{(1-f)h}{\tau_{21}} + \frac{f(1-h)}{\tau_{12}} \tag{7}$$

$$\frac{\partial f}{\partial t} = \frac{(1-f)h}{\tau_{21}} - \frac{f(1-h)}{\tau_{12}} - \frac{f^2}{\tau_{1R}} - S_{av}\Gamma\frac{g_{max}(\hbar w_p)}{N_Q}(2f-1)L\frac{c}{n_g} \tag{8}$$

where q is the electron charge, L_w is the effective thickness of the active layer, Γ is the optical confinement factor and N_Q is the surface density of QDs. The average signal photon density S_{av} is given by [14]

$$S_{av} = \frac{g_sP_{in}n_g}{\hbar w_pL_wDLg_{max}c} \tag{9}$$

P_{in} is the input signal power to the SOA, n_g is the group refractive index, $\hbar$ is the normalized Plank's constant, w_p is the peak frequency, D is the strip width, L is the cavity length, c is the free space light speed, g_{max} is the peak material gain taken at the peak frequency. The input signal wavelength is assumed to be injected to the QD SOA at a peak wavelength of GS for each structure. The single-pass gain of the structure is given by [11]

$$g_s = \exp\left[\left(g_{max}\Gamma - a_{int}\right)L\right] \tag{10}$$

where a_{int} is the loss coefficient. Although WL is assumed here to receive carriers by current injection or by escapes from QD ES, but the three RE models consider it as a common reservoir [10, 15]. From the architecture of these three RE model, ES works as a common reservoir since it receives carriers from the states above and below it (WL and GS, respectively). So, ES is referred to as a reservoir for GS [8]. This is contradicted with the experimentally evidenced that carriers stay long in WL and short in ES [16]. Due to this and other reasons, discussed below, four REs system is more appropriate.
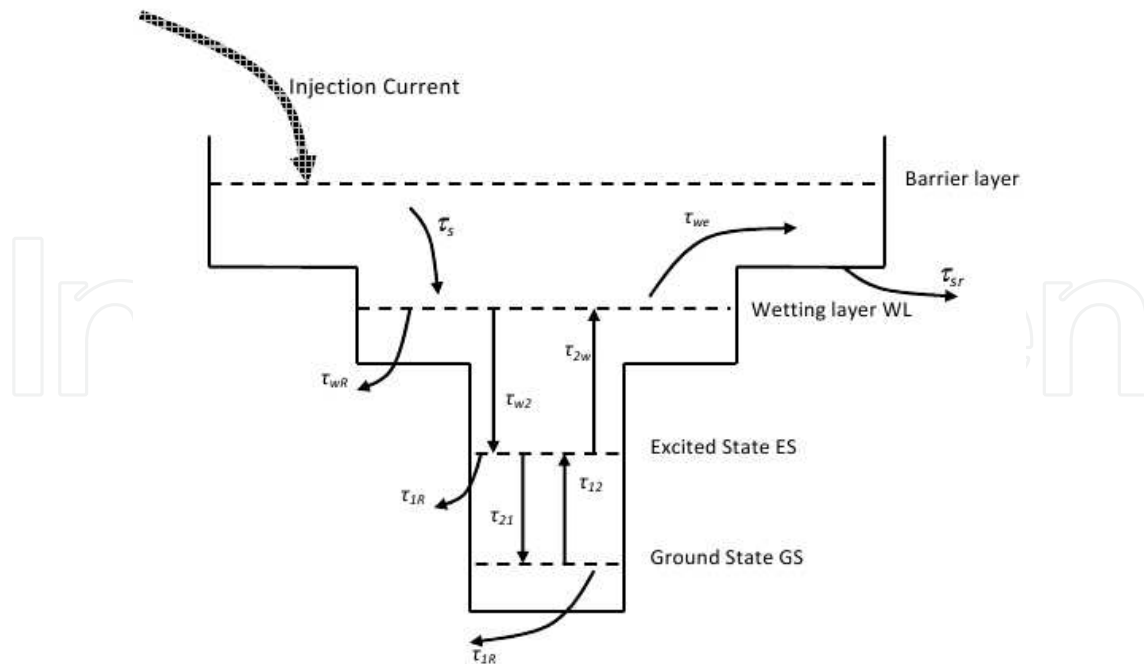
Fig. 2. Energy diagram of QD-SOA system.

5.2 Four rate equations model

Four REs system is used here to study Sb-based QD-SOAs and is built depending on the energy band diagram considered in Fig. 2. The advantages of using four rate equations system are twofold: 1) including of SCH barrier layer dynamics which is important in practice and 2) this RE model is more appropriate with the use of global Fermi-energy in the gain calculations which is described in section 2. In this four REs system, carriers are assumed to be injected with current density, J, in the SCH barrier layer then recombine at a rate $(1/\tau_{sr})$, relax at rate $(1/\tau_s)$ to the WL which works as a common reservoir for the carriers. The escape rate from WL to the SCH is $(1/\tau_{we})$. Other processes are described in section 5.1. The processes in the four REs system are represented by the following REs model which covers carrier density, N_s, in SCH barrier layer, in addition to: N_w, h and f which are covered also in the three REs model

$$\frac{\partial N_s}{\partial t} = \frac{J}{qL_w} - \frac{N_s}{\tau_s} - \frac{N_s}{\tau_{sr}} + \frac{N_w}{\tau_{we}} \tag{11}$$

$$\frac{\partial N_w}{\partial t} = \frac{N_s}{\tau_s} - \frac{N_w(1-h)}{\tau_{w2}} + \frac{N_w h}{\tau_{2w}} - \frac{N_w}{\tau_{wR}} - \frac{N_w}{\tau_{we}} \tag{12}$$

$$\frac{\partial h}{\partial t} = \frac{N_w L_w(1-h)}{N_Q \tau_{w2}} - \frac{N_w L_w h}{N_Q \tau_{2w}} - \frac{(1-f)h}{\tau_{21}} + \frac{f(1-h)}{\tau_{12}} \tag{13}$$

$$\frac{\partial f}{\partial t} = \frac{(1-f)h}{\tau_{21}} - \frac{f(1-h)}{\tau_{12}} - \frac{f^2}{\tau_{1R}} - S_{av}\Gamma \frac{g_{max}(\hbar w_p)}{N_Q}(2f-1)L\frac{c}{n_g} \tag{14}$$

Quasi-thermal equilibrium is assumed between states. To ensure this convergence, the carrier escape times are related to the carrier capture times as follows [17]

$$\tau_{12} = \tau_{d0}(\mu_{GS} / \mu_{ES})e^{([E_{ES}-E_{GS}]/k_BT)} \tag{15}$$

$$\tau_{2w} = \tau_{c0}(\mu_{ES}N_Q / \rho_{weff})e^{([E_{wl}-E_{ES}]/k_BT)} \tag{16}$$

$$\tau_{we} = \tau_s(\rho_{weff}N_{QD} / \rho_{SCH}H_b)e^{(\Delta E_{SCH,wl}/k_BT)} \tag{17}$$

GS and ES QD energy levels are denoted by E_{GS}, E_{ES}. ρ_{weff} is the density of states per unit area in the WL and ρ_{SCH} is the density of states per unit volume in the SCH. They are given by $\rho_{weff} = (m_{ewl}k_BT / \pi\hbar^2)$ and $\rho_{SCH} = 2(2m_{eSCH}\pi k_BT / \hbar^2)^{3/2}$. N_{QD} is the number of QD layers and H_b is the total thickness of the SCH. $\Delta E_{SCH,wl}$ is the energy difference between SCH and WL band edge energies. The capture times τ_{c0} and τ_{d0} are the average capture time from the WL to the ES and from the ES to the GS with the hypothesis that the final state is empty.

6. Sb-based QD-SOA structures

Sb-based QD semiconductors suffer from the difficulty of QD growth methods, like the self-assembled growth method, due to kinetic effects. Sb-based QD crystals growth hinders due to large mismatch (>7 or 8%) with GaAs semiconductors. Now it is possible to grow GaSb QDs on GaAs substrate [18]. In addition, an interfacial misfit array method can be used now to grow Sb-based layers on a GaAs platform although the (8%) lattice mismatch between GaAs and GaSb [19].

Accordingly, we choose a large number of structures, it is classified here in a five types, as in Table 1. In these structures, we change the composition of QD (structure Nos. 1, 4 and 5), WL (No. 2) or barrier layer (No. 3). This is to examine the effect of these layers on the QD-SOA and also to specify the possible spectral ranges in the Sb-based QD structures. In all of these structures there is a lattice mismatch between layers (dot and WL or WL and barrier) not exceeds (6%) and in some cases its value is very small. This is to intend these structures to the ease of QD growing. QD energy levels are calculated using parabolic band quantum-disc model [20] where the dots are assumed to be in the form of a disc with radius $(14\,nm)$ and height $(h = 2\,nm)$, unless states otherwise. Quantum well WL thickness is taken as (9 nm). The accuracy of the quantum disc model is checked by a comparison with the experimental data and numerical methods [20, 21]. The parameters used in the calculations of Sb-based structures are stated in Tables 2 and 3. Thus, it is adequate to calculate energy levels without time consumption. An example of QD energy levels calculated using parabolic band model is shown in Fig. 3 for InAs$_{0.1}$Sb$_{0.9}$ /GaAs$_{.1}$Sb$_{.9}$/Al$_{.1}$Ga$_{.9}$As QD-SOA. In the calculation of quasi-Fermi energy Eqs. (3) and (4) are used. Gain is then calculated, using Eq.1, and its peak value and peak wavelength for each structure is specified.

No.	Structure	No.	Structure
1	InAs$_x$Sb$_{1-x}$/GaAs$_{0.1}$Sb$_{0.9}$/Al$_{0.1}$Ga$_{0.9}$As	4	GaSb/GaAs$_{0.7}$Sb$_{0.3}$/GaAs
2	In$_{0.1}$AsSb$_{0.9}$/GaAs$_x$Sb$_{1-x}$/Al$_{.1}$Ga$_{.9}$As	5	InSb/GaAs$_{0.7}$Sb$_{0.3}$/GaAs
3	In$_{0.1}$AsSb$_{0.9}$/GaAs$_{0.1}$Sb$_{0.9}$/Al$_x$Ga$_{1-x}$As		

Table 1. QD-SOA structures studied.

Parameter	Symbol (Unit)	InSb	GaSb	InAs	GaAs
Bandgap energy	E_g (eV)	0.17	0.73	0.36	1.424
Electron Effective Mass	m_e^* / m_0	0.0145	0.044	0.022	0.065
Heavy-hole Effective mass	m_{hh}^* / m_0	0.44	0.33	0.41	0.45
Refractive index	n	4	3.82	3.52	3.65

Table 2. Binary structure parameters [22].

Structure	Relation
$InAs_xSb_{1-x}$	$E_g(InAs_xSb_{1-x}) = 0.18 - 0.41x + 0.58x^2$ $m_i(ABC) = m_i(AC) + m_i(BC)$
$GaAs_xSb_{1-x}$	$E_g(GaAs_xSb_{1-x}) = 0.726 - 0.502x + 1.2x^2$ $m_i(ABC) = m_i(AC) + m_i(BC)$
$Al_xGa_{1-x}As$	$E_g(Al_xGa_{1-x}As) = 1.242 + 1.247x$ $m_i(ABC) = m_i(AC) + m_i(BC)$

Table 3. The relation used to calculate structure parameters (bandgap E_g and effective mass m_i). Note that the subscript (i) with m_i refers to conduction or valence band effective masses [22, 23].

AlGaAs Barrier

GaAs$_{0.1}$Sb$_{0.9}$ WL

E$_{cWL}$=0.846eV

ΔEc =0.35 eV

E$_{c2}$=0.5592eV

E$_{c1}$=0.3846eV

E$_{gBarrier}$=1.549 eV

E$_{gWL}$=0.688 eV

E$_{gQD}$ =0.145eV

InAs$_{0.1}$Sb$_{0.9}$ QD

E$_{HH1}$=-0.0965eV
E$_{HH2}$=-0.1142eV
E$_{HH3}$=-0.1409eV

ΔEv=0.22 eV

E$_{HHWL}$=-0.6543eV
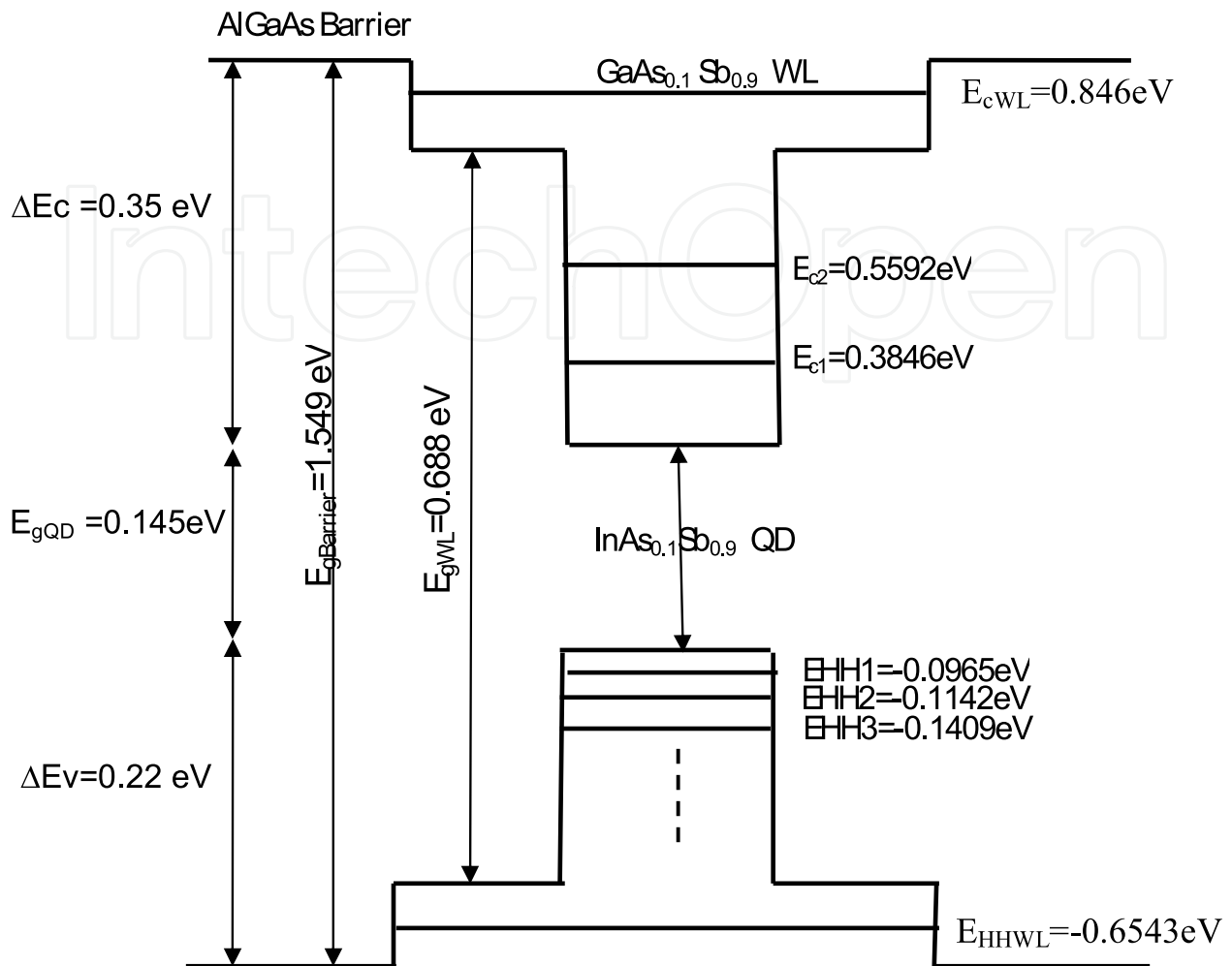
Fig. 3. Energy band diagram of an InAs$_{0.1}$Sb$_{0.9}$/GaAs$_{0.1}$Sb$_{0.9}$/Al$_{0.1}$Ga$_{0.9}$As QD-SOA structure.

7. Simulation results and discussion

7.1 QD-SOA gain

The REs system are solved numerically to see the gain change with input power P_{in}, and to examine the dynamic effects. The parameters used in the numerical calculations are listed in Table 4. Fig. 4 shows input power-gain curves for Sb-based QD-SOAs studied. Fig. 4 (a) shows the effect of changing Sb mole fraction in the QD layer. The effect of WL, barrier and QD layers composition on gain is shown in Fig. 4 (b), (c), (d). Curve arrangement in these figures coincides with that in [12]. While both QD and WL composition are shown to give a respected changes in gain, the contribution due to changing Sb-composition in the barrier layer is minor as in Fig. 4 (c). The overall behavior of Fig. 4 is the same, gain saturates at low input power, then it declines at high input powers. This can be attributed to the carrier depletion in the QDs where the output power begins to increase. In Fig. 4 (d), InSb QD-SOA gives a higher gain than that obtained from GaSb QD-SOA. Comparing Fig. 4 (a) and (d) shows the effect of QD composition. To deal with composition effect, we must refer to the material confinement effect: the difference between bandgap in the dot and WL. The higher difference gives more carrier confinement in the QD layer. InSb is known as a lower band

Parameter	Symbol	Value	Unit
Spontaneous radiative lifetime in QDs	τ_{1R}	0.4	ns
Spontaneous radiative lifetime in WL	τ_{wR}	1	ns
Carrier escapes time from ES to WL	τ_{c0}	1	ps
Carrier relaxation time from the two-dimensional WL to the ES	τ_{w2}	3	ps
Carrier relaxation time from GS to ES	τ_{12}	1.2	ps
Carrier relaxation time from ES to GS	τ_{d0}	7	ps
Diffusion time in the barrier layer	τ_s	6	ns
SCH recombination time	τ_{sr}	4.5	ns
Internal loss	α_{int}	2	cm^{-1}
Optical confinement factor	Γ	0.007	
Laser length	L	2000	μm
Strip . width	D	10	μm
The effective thickness of the active layer	L_w	0.1	μm
Injection current density	J	1.335	kA/cm^2

Table 4. Parameters used in the calculations [11, 17].

gap semiconductor. Thus, a higher gain is obtained from InSb than GaSb QD-SOAs due to the higher material confinement of the former (GaSb bandgap differ from InSb by ~0.56 eV). This reason is not enough to explain curves arrangement in Fig. 4 (a). Here gain curves are not arranged due to QD band gap where only very small differences result from varying Sb mole fraction in the QD region. Thus, in addition to material confinement, one must refer to the quantum confinement. Curves are arranged due to the gap $(E_{c1}+E_g+E_{v1})$ where E_{c1}, E_{v1} are the 1st conduction and valence subbands and E_g is the QD band gap. From Figs. 4 (a) and (d), the structure $InSb/GaAs_{0.7}Sb_{0.3}/GaAs$, is more appropriate for inline static amplification applications due to its maximum gain obtained and higher saturation power than $InAs_xSb_{1-x}/GaAs_{0.1}Sb_{0.9}/Al_{0.1}Ga_{0.9}As$ and GaSb QD-SOAs. The effect of QD size is shown in Fig. 4 (e) and (f). In Fig. 4 (e), it is shown that QDs with shorter height gives a higher gain. In Fig. 4 (f), QDs with longer radius gives higher gain.
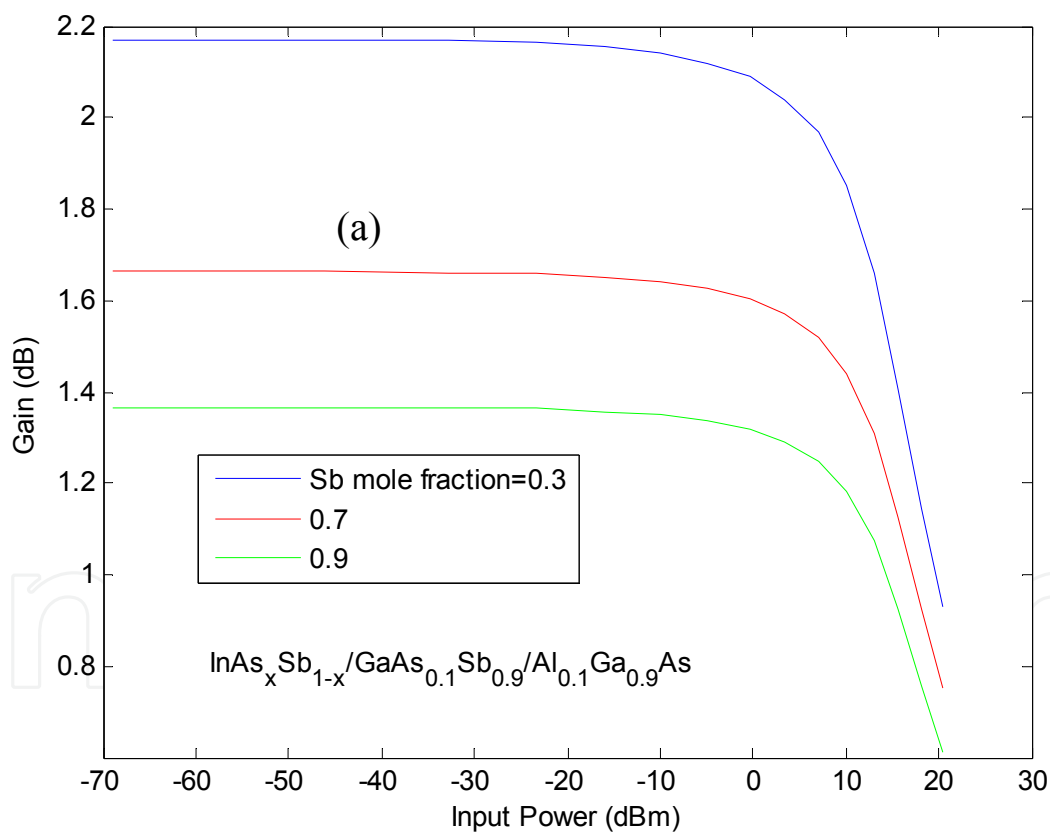
Fig. 4. (Continued)
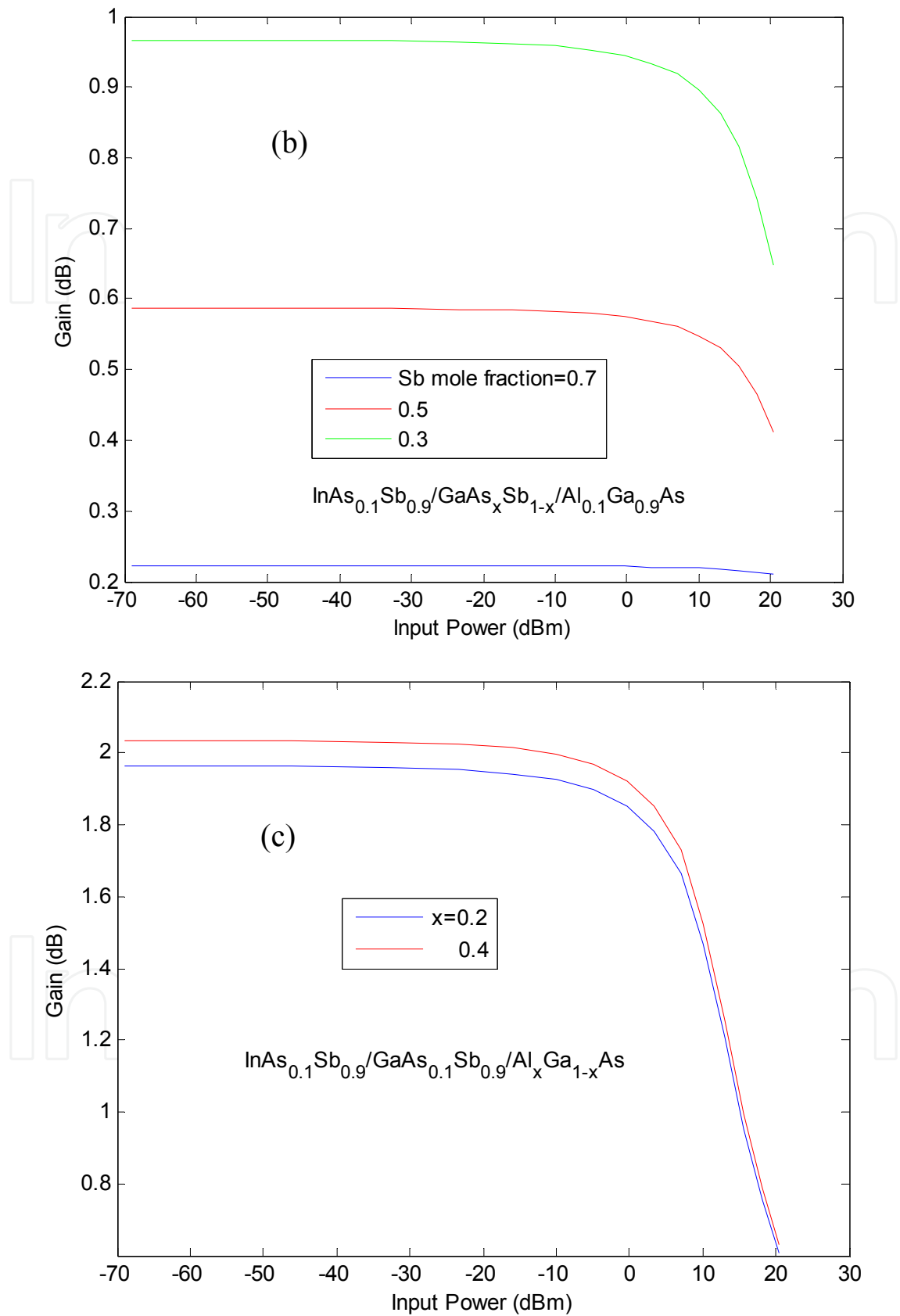
Fig. 4. (Continued)
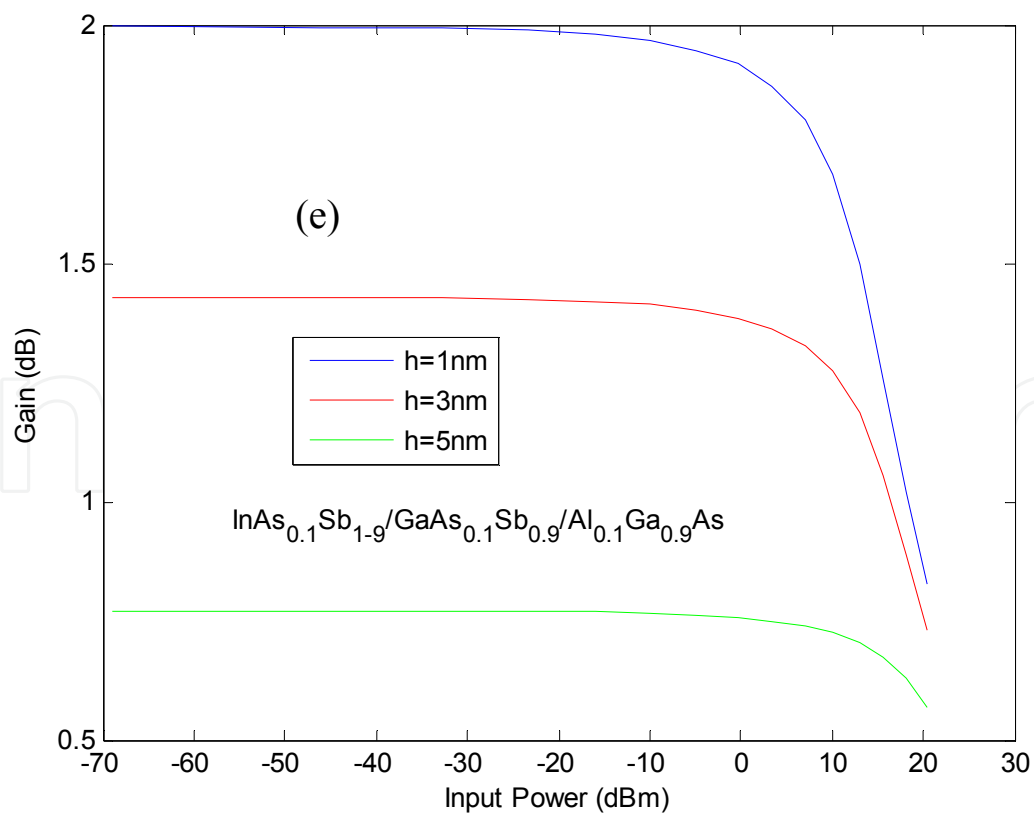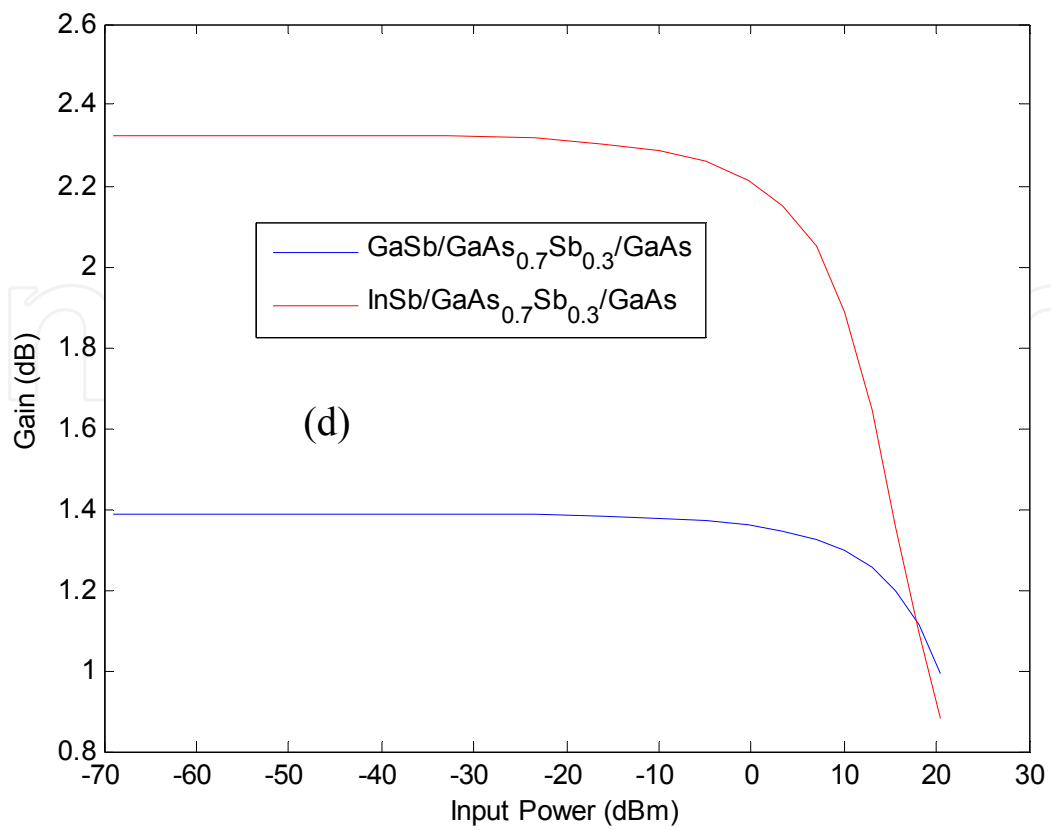
Fig. 4. (Continued)
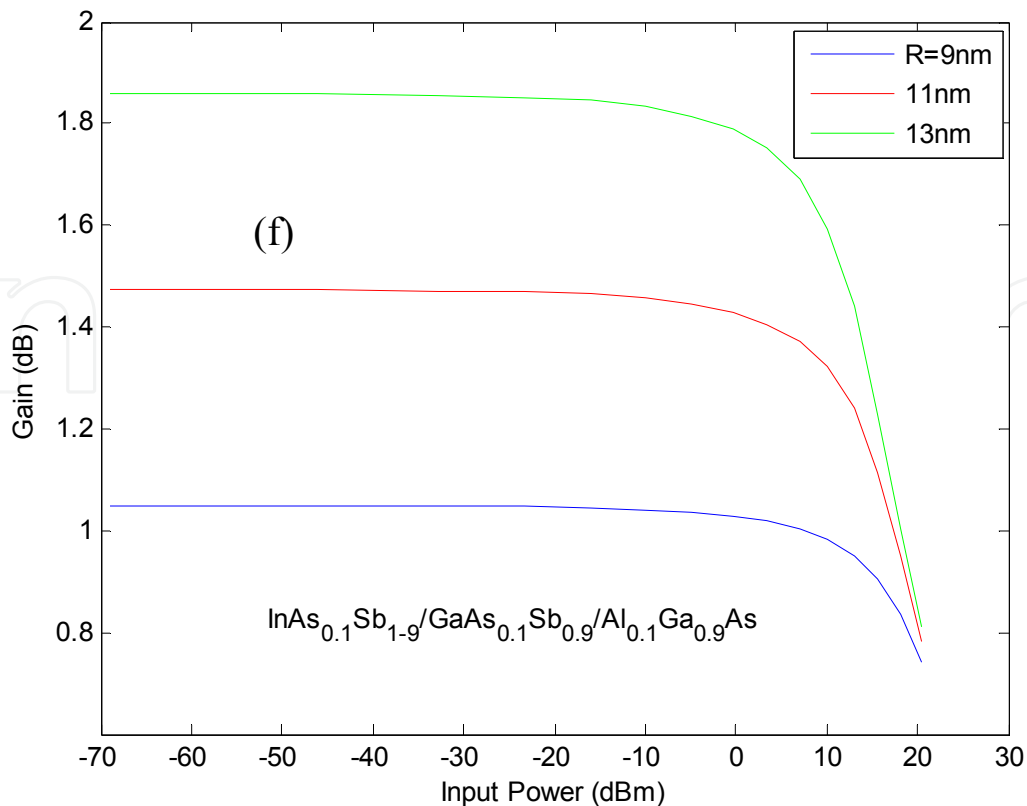
Fig. 4. Gain-input power relation at J=1.335 kA/cm² for the QD-SOAs: (a) $InAs_xSb_{1-x}$/$GaAs_{0.1}Sb_{0.9}$/$Al_{0.1}Ga_{0.9}$, (b) $InAs_{0.1}Sb_{0.9}$/$GaAs_xSb_{1-x}$/$Al_{0.1}Ga_{0.9}As$, (c) $InAs_{0.1}Sb_{0.9}$/$GaAs_{0.1}Sb_{0.9}$/ $Al_xGa_{1-x}As$, (d) GaSb and InSb. (e) The disc height and (f) the disc radius for $InAs_{.1}Sb_{.9}$/$GaAs_{.1}Sb_{.9}$/$Al_{.1}Ga_{.9}As$ QD-SOA is shown.

7.2 Dynamical effects

Figure 5 (a) shows the carrier density dynamics in the barrier layer N_s of $InAs_xSb_{1-x}$/$GaAs_{.1}Sb_{.9}$/$Al_{.1}Ga_{.9}As$ QD-SOAs at three x-mole fraction values (x=0.3, 0.7 and 0.9 Sb-fraction). The energy subbands of the QD at each mole fraction are included through relaxation times (see Eqs. 15-17), thus a difference appears between curves. The carrier density in the barrier layer obtained here is in the range of (10^{15}cm⁻³) which is near to the value of WL carrier density in [11] which assumes that carriers are injected directly to WL. N_s curves are arranged according to the shallower Fermi energy level in the barrier layer of the QD SOA structure. According to this, the barrier layer in the structure with (0.9) Sb mole fraction filled earlier, since its quasi-Fermi energy is shallower, then the structure with (0.3) and finally, the structure with (0.7) Sb mole fraction. Fig. 5 (b) shows the carrier density in the WL (N_W). While N_W obtained here is in the range of (10^{12}cm⁻³), a (10^{14} - 10^{15} cm⁻³) WL carrier density is obtained in [11] due to the neglect of barrier layer in that work. Here, N_W curves are arranged according to the quasi-Fermi energy in their wetting layers. Fig. 5 (c) and (d) shows ES and GS occupation probabilities for the structures $InAs_xSb_{1-x}$/$GaAs_{.1}Sb_{.9}$/$Al_{.1}Ga_{.9}As$ at Sb mole fractions (0.3, 0.7 and 0.9) where the same probability is obtained in these structures for each ES and GS. This is due to very small differences between their relaxation times, i.e. the inclusion of QD subbands energies, not so much effects, see Eqs. (15-17). In Fig. 6 (a), the effect of changing mole-fraction in the WL of $InAs_{.1}Sb_{.9}$/$GaAs_xSb_{1-x}$/$Al_{.1}Ga_{.9}As$ QD structure is studied. WL is shown to be saturated at
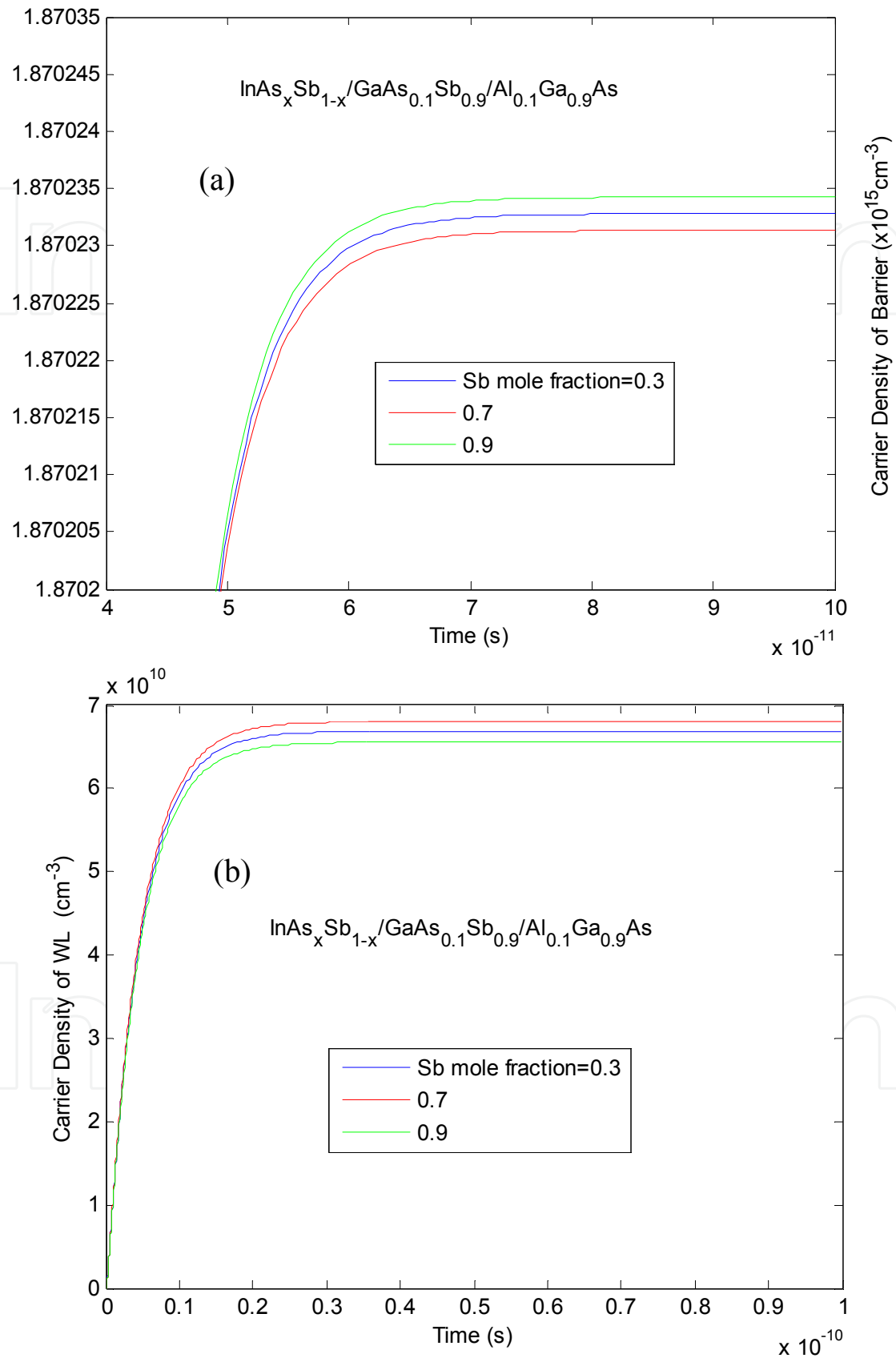
Fig. 5. (Continued)
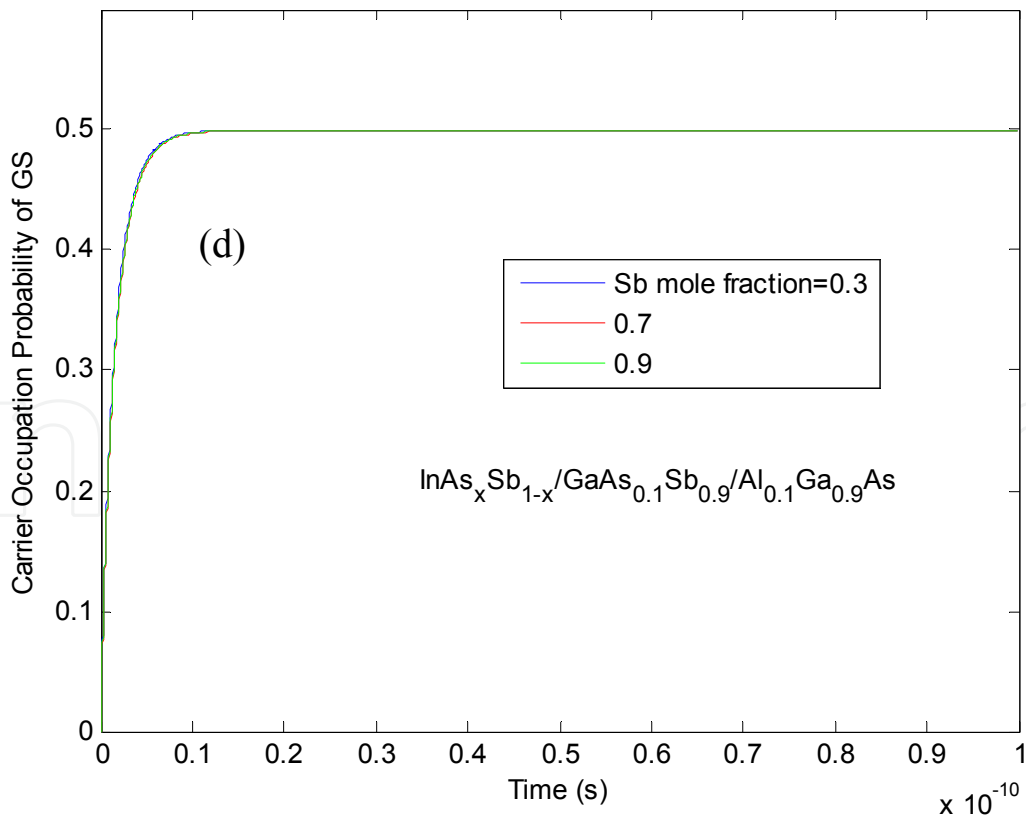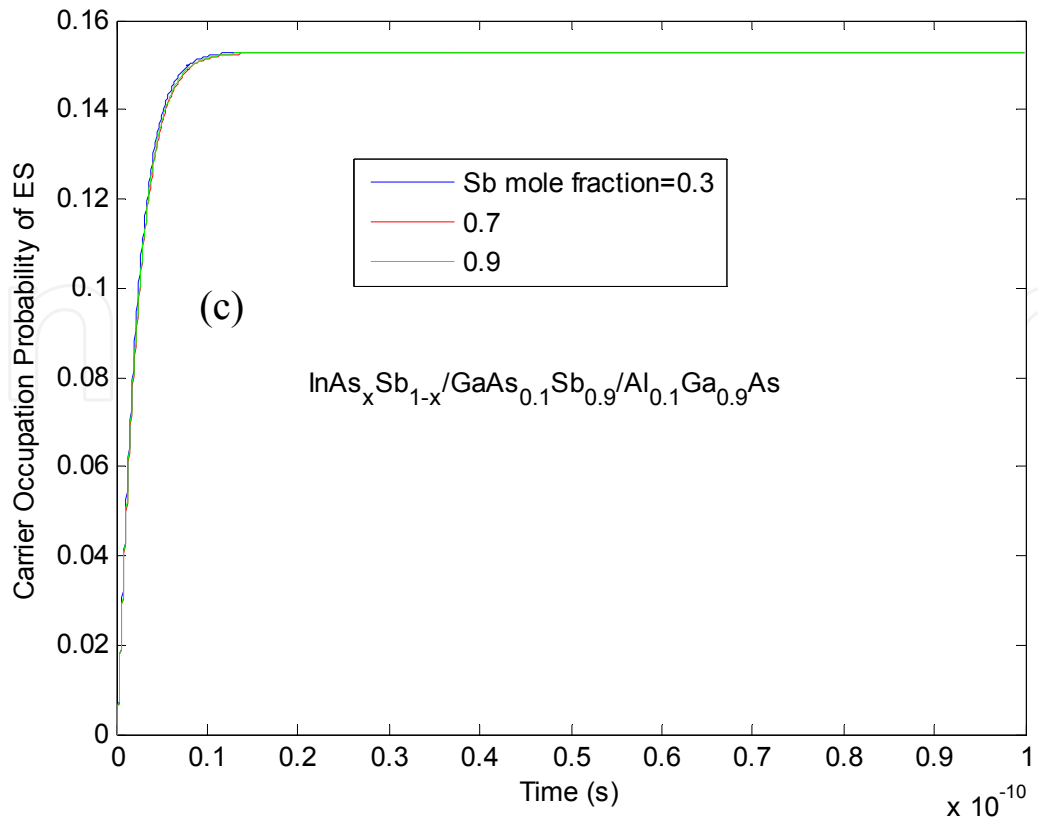
Fig. 5. Carrier density for (a) barrier and (b) WL. Then occupation probability for (c) ES, and (d) ES for InAs$_x$Sb$_{1-x}$/GaAs$_{0.1}$Sb$_{0.9}$/Al$_{0.1}$Ga$_{0.9}$As QD-SOAs.

higher carrier density for the structures with Sb mole fraction in WL (0.3 and 0.5). Here curves arrangement is appear according to shallower quasi-Fermi energy levels in the WL, where the effect of WL band gap energy is obvious in this arrangement. Fig. 6 (b) and (c) shows the dynamics of ES and GS occupation probabilities, respectively. Checking the parameters that arrange these curves shows that although the escape times to ES (τ_{12} and τ_{2w}) are very short for the structure No. 2 with Sb mole fraction (0.7), it saturates after other mole fractions (0.3 and 0.5) in these structures. This can be explained if one follows the energy difference between QD ES and WL energy level where this difference is greater for the structure with (0.7) Sb mole fraction in the WL. Also for GS one must refer to the difference between QD GS subband and WL energy level. In Fig. 7, the WL dynamics are shown for $In_{0.1}AsSb_{0.9}/GaAs_{0.1}Sb_{0.9}/Al_xGa_{1-x}As$ QD-SOAs. WL carrier density saturates at a higher value for the structure with (x=0.2) Al mole fraction in the barrier layer. Also the same reason for shallower quasi-Fermi energy in the WL can explain this arrangement. One can refer to effect of the main difference between structures here (energy gap of barrier layer E_{gb}) where a higher separation between N_W curves is compared to the effect of WL energy gap (E_{gw}) as shown in Fig. 6 (a). Occupation probabilities in GS and ES coincides for both (x=0.2 and 0.4) structures and thus they are not drown. In Figs. (5)-(6), although the faster rate of transition between ES and GS, but they are not always the faster one reaching steady state. Both SCH barrier and WL get steady state faster although there is a longer rate of transition between the barrier and WL. This is because of the limited dynamics for these layers so they are in the steady state earlier. At all cases, the GS reaches steady state faster
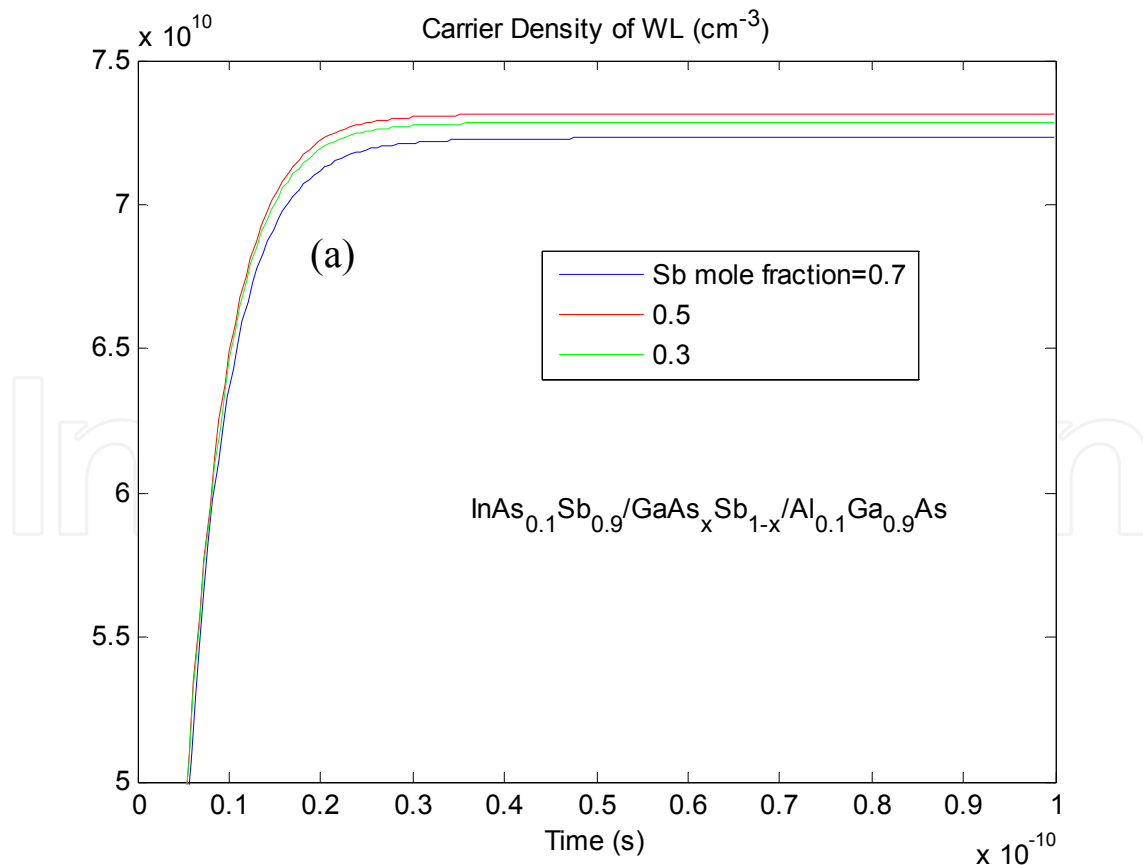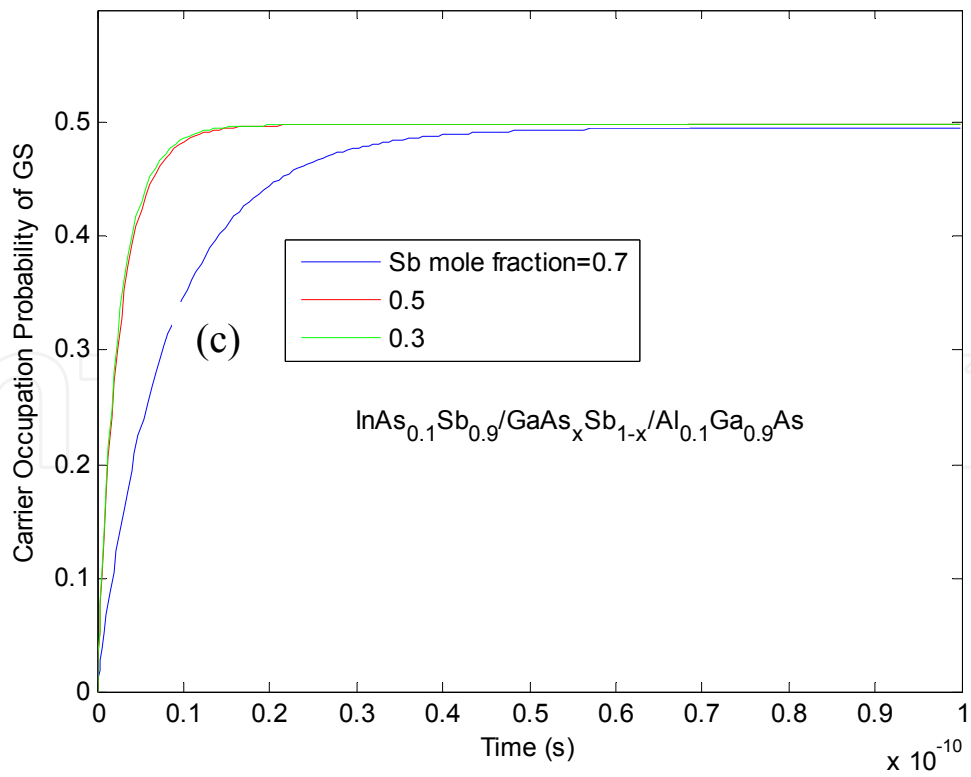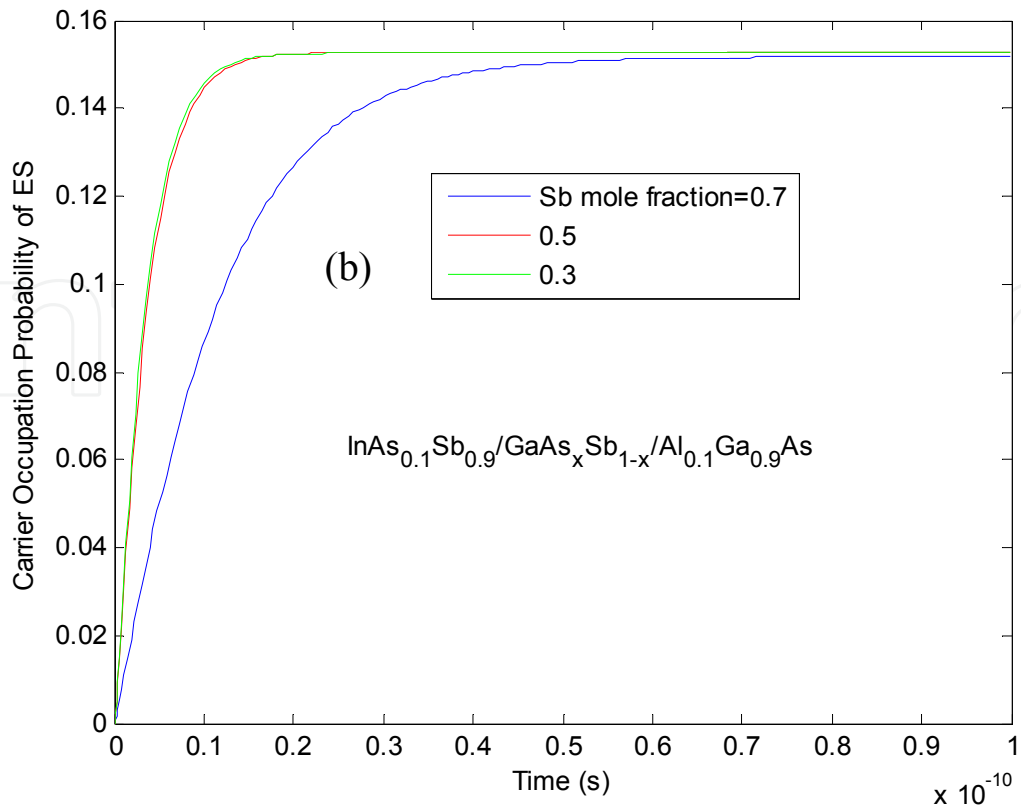

Fig. 6. (Continued)

Fig. 6. (a) Carrier density for WL. Then occupation probability for: (b) ES and (c) GS for InAs$_{0.1}$Sb$_{0.9}$/GaAs$_x$Sb$_{1-x}$/ Al$_{0.1}$Ga$_{0.9}$As QD-SOAs

than ES since the relaxation between ES to GS is very fast. Finally, a comparison is done between three and four REs system for QD-SOA as shown in Fig. 8 (a), (b) and (c) for WL, ES and GS respectively, where a three REs system is shown to be an overestimates the dynamics due to neglecting the effect of barrier layer. So, this layer must be included in the REs system used to study QD systems.
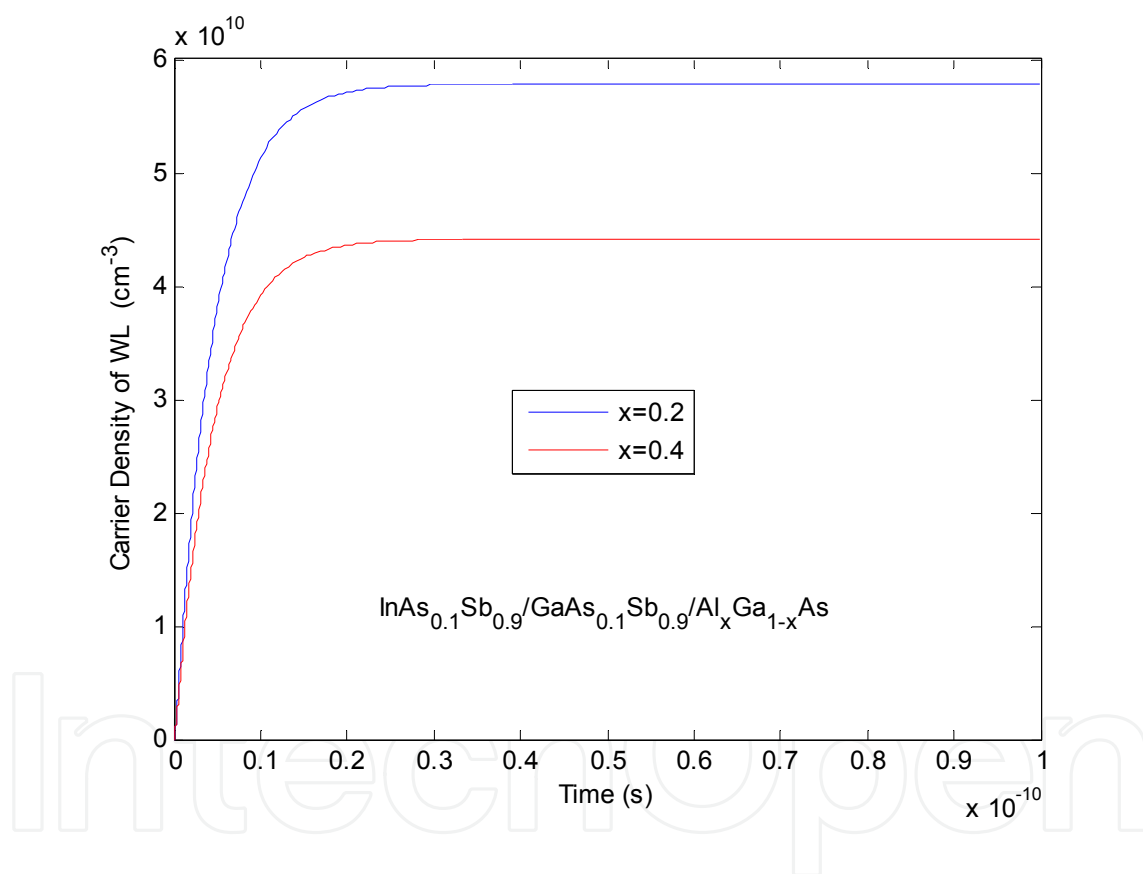
Fig. 7. Carrier density for WL for $InAs_{0.1}Sb_{0.9}/GaAs_{0.1}Sb_{0.9}/Al_xGa_{1-x}As$ QD-SOAs.
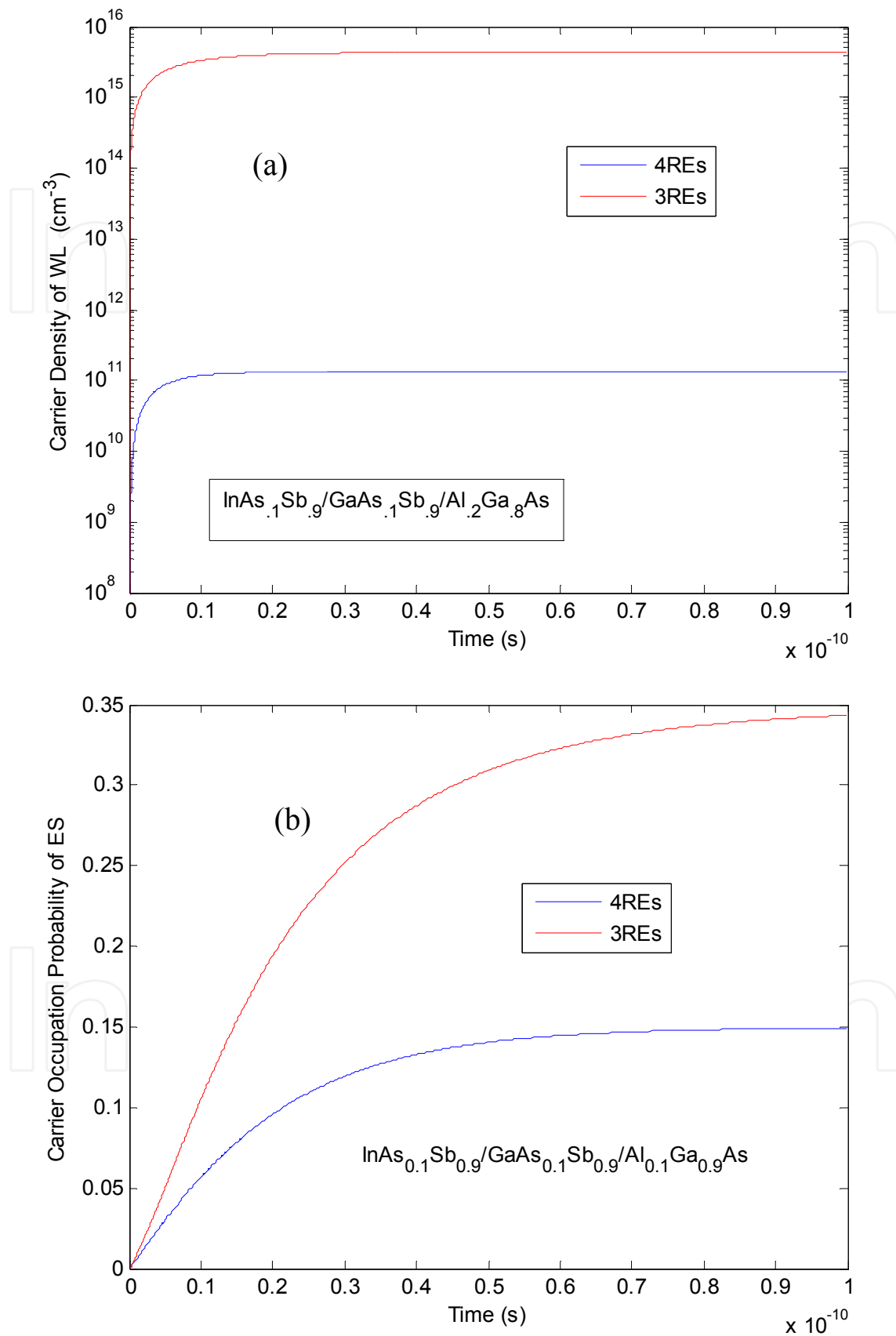
Fig. 8. (Continued)
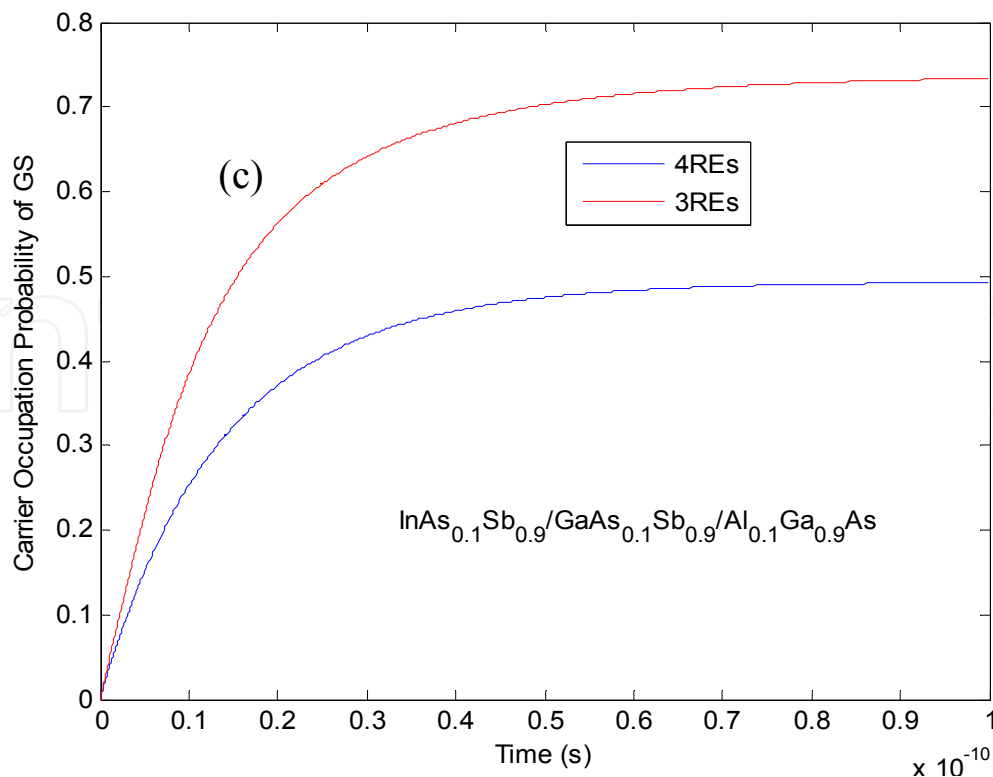
Fig. 8. A comparison between three- and four-REs system for (a) WL carrier density, (b) ES and (c) GS occupation probabilities for InAs$_{.1}$Sb$_{.9}$/GaAs$_{.1}$Sb$_{.9}$/Al$_{.1}$Ga$_{.9}$As QD-SOA.

8. Conclusions

The progress towards SOAs, and then QD-SOAs, is reviewed. The importance of Sb-based structures is illuminated. To see the effect of QD-SOA layers, a REs for QD, WL and SCH layers are solved numerically. This make us specify gain-input power relation for Sb-based QD-SOAs and then examine layers dynamics. Both QD and SCH layers are shown to have an importance in the static characteristics due to their considerable effect in structure confinement. WL is shown to affect carrier dynamics especially in the ES and GS. Global quasi-Fermi energy (which included SCH, WL, QD ES and QD GS) is shown to be important in the explanation of results. At all cases, the inclusion of the SCH in the REs is shown to be essential.

9. Acknowledgment

10. References

[1] Weng W. Chow and Stephen W. Koch, Semiconductor Laser: Fundamentals (Berlin, Springer, 1999), 1.

[2] Scott W. Corzine, Ran-Hong Yan and Larry A. Coldren, "Optical Gain in III-V Bulk and Quantum Well Semiconductors," in Quantum Well Lasers, ed. Peter S. Zory (New York, Academic Press, 1993), 18.

[3] Y. Ben Ezra, B. I. Lembrikov and M. Haridim, "Ultrafast all-optical processor based on quantum-dot semiconductor optical amplifiers," IEEE J Quantum Electronics 45, no. 1 (2009): 34.

[4] Michael J. Connelly, Semiconductor optical amplifier, (New York, Kluwer academic publishers, 2002), 3.

[5] Baqer Al-Nashy, Static and dynamic characteristics of Sb-based quantum-dot semiconductor optical amplifiers, a thesis, (Baghdad-Iraq, Baghdad University, 2010), 6.

[6] H. Shao and others, "Room Temperature InAsSb Photovoltaic Detectors for Mid-Infrared Applications," IEEE Phot. Tech. Lett., 18, no. 16 (2006): 1756.

[7] R. Sidhu, N. Duan, J. C. Campbell, and A. Holmes, "A Long-Wavelength Photodiode on InP Using Lattice-Matched GaInAs–GaAsSb Type-II Quantum Wells," IEEE Phot. Tech. Lett. 17, no. 2 (2005): 2715.

[8] G. Liu and Shun-Lien Chuang, "Modeling of Sb-based type-II quantum cascade lasers," Phys. Rev. B 65 (2002): 165220.

[9] Jungho Kim and others, "Static gain saturation model of quantum-dot semiconductor optical amplifiers," IEEE J. Quantum Electron. 44, no. 7 (2008): 658.

[10] Baqer Al-Nashy and Amin H. Al-Khursan, "Linear and nonlinear gain of Sb-based quantum-dot semiconductor optical amplifiers," Recent Patents on Electrical Engineering, 3, no. 3 (2010): 232.

[11] Y. Ben Ezra, B. I. Lembrikov, and M. Haridim, "Specific Features of XGM in QD-SOA," IEEE J. Quantum Electron. 43, no. 8 (2007): 730.

[12] Baqer Al-Nashy and Amin H. Al-Khursan, "Completely inhomogeneous density-matrix theory for quantum-dots", Optical and Quantum Electronics, 41, 989-995, 2010.

[13] Dieter Bimberg and others, "InGaAs-GaAs quantum dot lasers," IEEE J. Selected Top. Quantum Electronics 3, no. 2 (1997): 196.

[14] M. Vasileiadis and others, "Potential of InGaAs/GaAs quantum dots for applications in vertical cavity semiconductor optical amplifiers," IEEE J. Quantum Electronics 14, no. 4 (2008): 1180.

[15] D. W. Reschner, E. Gehrig and O. Hess, "Pulse amplification and spatio-spectral hole-burning in inhomogeneously broadened quantum-dot semiconductor optical amplifier," IEEE J. Quantum Electronics 45, no. 1 (2009): 21.

[16] Y. Ben-Ezra, B. I. Lembrikov, and M. Haridim, "Acceleration of gain recovery and dynamics of electrons in QD-SOA," IEEE J. Quantum Electronics 41, no. 10 (2005) 1268.

[17] Jin-Long Xiao and Yong-Zhen Huang, "Numerical Analysis of Gain Saturation, Noise Figure, and Carrier Distribution for Quantum-Dot Semiconductor-Optical Amplifiers," IEEE J. Quantum Electronics 44, no. 5 (2008): 448.

[18] P. Mock and others, "MOVPE grown self-assembled Sb-based quantum dots assessed by means of AFM and TEM," IEE Proc.-Optoelectronics 147, no. 3 (2000): 209.

[19] M. Mehta, A. Jallipalli, J. Tatebayashi, M. N. Kutty, A. Albrecht, G. Balakrishnan, L. R. Dawson, and D. L. Huffaker, "Room-Temperature Operation of Buffer-Free GaSb–AlGaSb Quantum-Well Diode Lasers Grown on a GaAs Platform Emitting at 1.65 μm," IEEE Phot. Tech. Lett. 19, no. 13 (2007) 1628.

[20] Amin H. Al-Khursan, M. Al-Khakan, K. Al-Mossawi, "Third-order non-linear susceptibility in a three-level QD system," Photonics and Nanostructures – Fundamentals and Applications 7, no. 3 (2009): 153.

[21] H. Al-Husseini, Amin H. Al-Khursan, S. Al-Dabagh, "III-nitride QD lasers", Open Nanosci. J. 3, (2009): 1.

[22] Wei Zhang and M. Razeghi, "Antimony-Based Materials forElectro-Optics," in Semiconductor nanostructures for optoelectronic applications, ed. Todd Steiner, (Boston, Artech House, 2004) 229.

[23] Shun-Lien Chuang, Physics of optoelectronic devices, (New York, J. Willy & sons, 1995), 708.
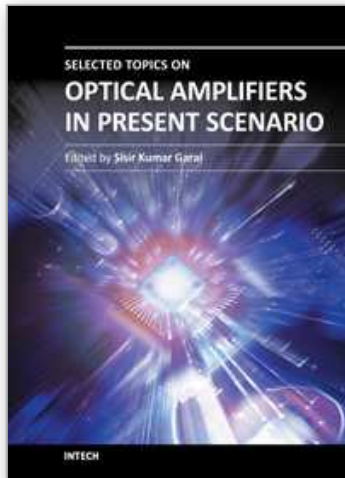
Selected Topics on Optical Amplifiers in Present Scenario

Edited by Dr. Sisir Garai

With the explosion of information traffic, the role of optics becomes very significant to fulfill the demand of super fast computing and data processing and the role of optical amplifier is indispensable in optical communication field. This book covers different advance functionalities of optical amplifiers and their emerging applications such as the role of SOA in the next generation of optical access network, high speed switches, frequency encoded all-optical logic processors, optical packet switching architectures, microwave photonic system, etc. Technology of improving the gain and noise figure of EDFA and, the study of the variation of material gain of QD structure are also included. All the selected topics are very interesting, well organized and hope it will be of great value to the postgraduate students, academics and anyone seeking to understand the trends of optical amplifiers in present scenario.

How to reference

In order to correctly reference this scholarly work, feel free to copy and paste the following:

B. Al-Nashy and Amin H. Al-Khursan (2012). The Composition Effect on the Dynamics of Electrons in Sb-Based QD-SOAs, Selected Topics on Optical Amplifiers in Present Scenario, Dr. Sisir Garai (Ed.), ISBN: 978-953-51-0391-2, InTech, Available from: http://www.intechopen.com/books/selected-topics-on-optical-amplifiers-in-present-scenario/the-composition-effect-on-the-dynamics-of-electrons-in-sb-based-qd-soas-

open science | open minds